International Journal of Pharmaceutics 702 (2026) 127193

Contents lists available at ScienceDirect

International Journal of Pharmaceutics

journal homepage: www.elsevier.com/locate/ijpharm

Scalable generation of droplet-templated amorphous solid dispersions using continuous antisolvent extraction

Jun Ho Min [a,b], Zheng Jie Liew [a,b], Leon Yoon Ho [b], Zhi Kai Tio [a,b], Arif Z. Nelson [c], Natalia Veronica [d], Lai Wah Chan [d], Paul Wan Sia Heng [d], Abigail Gershman [e], Samir Kulkarni [e], John Richard Murphy [f], Jennifer Ann Dolman [f], Catherine Michelle Ambler [g], Shawn LaCasse [e], Kapildev Arora [e], Saif A. Khan [a,*], Patrick S. Doyle [b,h,*]

[a] Department of Chemical and Biomolecular Engineering, National University of Singapore, 4 Engineering Drive 4, #02-09 Block E5, SG117585, Singapore
[b] Singapore-MIT Alliance for Research and Technology, 1 CREATE Way, #04-13/14 Enterprise Wing, SG 138602, Singapore
[c] Food, Chemical and Biotechnology Cluster, Singapore Institute of Technology, 10 Dover Dr, SG 138683, Singapore
[d] Department of Pharmacy and Pharmaceutical Sciences, GEA-NUS Pharmaceutical Processing Research Laboratory, National University of Singapore, 18 Science Drive 4, SG 117543, Singapore
[e] Pfizer Worldwide Research & Development, Pharmaceutical Sciences, Groton, CT 06340, USA
[f] Pfizer Global Research & Development, Pharmaceutical Sciences, Sandwich, Kent CT13 9NJ, UK
[g] Pfizer Global Research & Development, Pharmaceutical Sciences, La Jolla, CA 92121, USA
[h] Department of Chemical Engineering, Massachusetts Institute of Technology, 25 Ames St, Cambridge, MA 02142, USA

ARTICLE INFO

Keywords:
Microfluidics
Particle engineering
Step-emulsification
Amorphous solid dispersion
Powder properties
Powder rheology
Tablet formulation

ABSTRACT

Amorphous solid dispersion (ASD) is a widely used formulation strategy for improving the apparent solubility and oral absorption of poorly water-soluble drugs. However, established commercial ASD manufacturing processes often generate powders with broad particle size distributions, irregular morphology and poor powder flowability, all of which complicate downstream processing. In this work, we introduce a droplet-templated ASD manufacturing process that combines step-emulsification co-processing of a polymer and drug with continuous anti-solvent extraction to produce highly monodisperse ASD particles. We produce intermediate ASD drug powder products with favorable particle attributes, including high monodispersity, improved flowability, and compatibility with downstream tableting. In contrast with prior reports on microfluidic production, this process allows the production of sufficient quantities of powder to enable compression into drug products (tablets). The tablets thus produced meet stringent drug product specifications (tensile strength, extended supersaturation dissolution profile and residual solvent below ICH limits). These results demonstrate that droplet microfluidics, traditionally viewed as a small-scale process, can be leveraged as a promising alternative manufacturing platform for ASDs with industrially relevant throughput for high-value pharmaceutical products.

1. Introduction

In recent years, there has been a surge of interest in using amorphous forms of active pharmaceutical ingredients to overcome poor aqueous solubility exhibited in their crystalline form (Wilson et al., 2020). The spotlight on amorphous solid dispersions (ASDs) has intensified as 60–70% of newly manufactured drugs fall under the biopharmaceutics classification system (BCS) Class II and IV compounds (Lugtu-Pe et al., 2021). While Class II drugs have limited absorption due to poor solubility, Class IV drugs exhibit low bioavailability due to a combination of low solubility and permeability (Papich and Martinez, 2015). By leveraging on higher free energy and lower density of amorphous substances, ASD formulations of Class II and potentially Class IV drugs can enhance the bioavailability and therapeutic effects compared to their crystalline counterparts (Babu and Nangia, 2011; Surampalli et al., 2013).

Established ASD manufacturing techniques such as freeze drying, spray drying, and jet milling are energy-intensive and often produce

* Corresponding authors at: Singapore-MIT Alliance for Research and Technology (Critical Analytics for Manufacturing Personalized-Medicine), 1 CREATE Way, #04-13/14 Enterprise Wing, SG 138602, Singapore (P.S. Doyle).
E-mail addresses: saifkhan@nus.edu.sg (S.A. Khan), pdoyle@mit.edu (P.S. Doyle).

https://doi.org/10.1016/j.ijpharm.2026.127193
Received 13 May 2026; Received in revised form 16 June 2026; Accepted 12 July 2026
Available online 17 July 2026

polydisperse particles with large size distributions that can negatively affect dissolution and oral bioavailability (Chu et al., 2012). In addition, these processes suffer from recrystallization which has been reported in spray-dried materials processed under different temperatures and feed rates (Beyer et al., 2016). Converting the resulting powders into suitable dosage forms pose yet another challenge to the downstream processing, often requiring additives and secondary excipients such as lubricants to improve their physical properties for tableting (Pandi et al., 2020). Hot-melt extrusion (HME) has emerged as a more modern approach for cost-effective and high-throughput production of amorphous solid dispersions (ASDs) (Agrawal et al., 2015). However, the risk of thermal degradation of heat-sensitive active pharmaceutical ingredients (APIs) and copolymers often limit the applicability of HME. Co-precipitated amorphous dispersion (cPAD) is another emerging technology that involves mixing co-dissolved APIs and polymers with a fully miscible antisolvent under high shear, followed by thermal annealing to achieve excellent particle properties (Strotman and Schenck, 2021). Despite its advantages, the heat introduced during high-shear mixing and thermal annealing can promote crystallization of amorphous materials (Kumar and Suryanarayanan, 2022) and many processing challenges remain in preventing such recrystallization behavior of ASDs (Myślińska et al., 2023). More recently, droplet microfluidics has been explored as an alternative platform for co-processing APIs and excipients through droplet solidification via extractive crystallization (Shikha et al., 2022; Ng et al., 2022; Fortt et al., 2020). Although the scope of the studies does not extend to producing amorphous compounds, the absence of thermal treatment in the process, as well as the superior powder rheology of co-processed materials produced may suggest a potential avenue for droplet microfluidics in fabricating amorphous compounds with improved powder properties.

Droplet microfluidics has gained broad popularity in recent years due to its remarkable ability to create particles with a narrow and consistent size distribution (Chong et al., 2015). Having exceptional control over particle size and morphology is highly beneficial for the pharmaceutical industry due to its effect on flowability and hence processibility in the downstream manufacturing (Ekdahl et al., 2019). Amongst many microfluidic droplet generators, T-junctions (Schneider et al., 2011) and cross-junctions (Loo et al., 2016) are most commonly used, which leverage the viscous shear force exerted by the continuous phase on the dispersed phase in a single channel format. Hence, many attempts have been made to scale this system by arraying multiple single-channel generators in parallel to achieve the desirable throughput (Yadavali et al., 2018). However, fluctuations in the flow rates can broaden droplet size distributions and result in the formation of satellite droplets (Loo et al., 2016). Planar shear devices can thus be difficult to scale up in practice as droplet size at each junction is sensitive to the local flow rates in the parallelized network (Wu et al., 2021).

Step-emulsification has recently emerged as a particularly attractive route for scalable droplet generation with precise control over emulsion size and monodispersity (Amstad et al., 2016). Unlike shear-driven methods, step-emulsification leverages preferential wetting, in which the strong affinity of the continuous phase for the channel walls causes a 'pinching-off' effect on the dispersed phase flow (Lian et al., 2019). Droplet formation is driven by the difference in Laplace pressure when the liquid confined in a shallow channel expands into a spherical droplet upon entering a deeper reservoir through a step (Eggersdorfer et al., 2018). The droplet size can therefore remain largely independent of flow rates over a wide operating window for both dispersed and continuous phases, as long as the dispersed phase is depleted faster from the nozzle than it is refilled (Ofner et al., 2016). This insensitivity to flow rate fluctuations can significantly simplify the device design and operation for industrial scale-up (Stolovicki et al., 2017).

Step emulsification devices are typically fabricated from polydimethylsiloxane (PDMS) due to its rapid and cost-effective prototyping in laboratory settings (Stolovicki et al., 2017). However, the poor compatibility of PDMS with many organic solvents (Lee et al., 2004) limits its use in pharmaceutical applications. To address this issue, Ofner *et al.* were the first to fabricate a step-emulsification device in glass using photolithography followed by etching and bonding of two aligned glass pieces (Ofner et al., 2016). Their work demonstrated the feasibility of generating highly monodisperse droplets using pharmaceutical solvents at throughputs of 25 mL/h, far exceeding those of single-channel devices. If such high-throughput droplet generation can be coupled with a suitable process to produce pharmaceutical products, such as ASDs, it could enable a new paradigm for precise and compact commercial-scale pharmaceutical manufacturing– this is indeed what we seek to demonstrate in this study.

This paper presents an integrated process for generating monodisperse ASD microparticles by coupling a glass step emulsification device with a subsequent unit operation of continuous antisolvent extraction. The novelty of the present work extends beyond the use of microfluidics for co-processing polymeric materials with APIs, which is a well-established approach (Sharratt et al., 2021; Shi et al., 2023). Rather, the paper demonstrates the feasibility of an industrially relevant and scalable microfluidics-enabled manufacturing technique that entails continuous operation, controlled solvent extraction and improved powder attributes for robust downstream processing. We chose Felodipine (FLP) as a model API and hypromellose acetate succinate (HPMCAS) as a model excipient in our studies. In contrast to prior microfluidic studies, the process allows the production of sufficient quantities of powder to subsequently enable compression into oral solid dosage forms with suitable tensile strength, an extended supersaturation dissolution profile, and residual DMC below the reporting limit. In this work, we can process droplets into powders at a representative dispersed-phase flow rate of 0.9 mL/min. The device could also be operated at dispersed-phase flow rates up to 10 mL/min for droplet generation, corresponding to a projected ASD solids throughput of up to 720 g/day at 5% w/v solids loading. While the higher flow-rate operation was associated with a modest increase in droplet size, as shown in Supplementary Fig. S2, these results indicate the potential scalability of the microfluidic droplet-generation step. Further optimization of the downstream extraction and recovery process would be required to translate this projected droplet-generation throughput to end-to-end powder production.

2. Materials and methods

2.1. Fabrication of glass step-emulsification device

We present a method to construct the glass step-emulsification device using a borofloat 33 glass. The device is composed of two glass chips, each measuring 150 mm x 50 mm x 3 mm, that serve as the top and bottom pieces of the device. Photolithography was used to pattern 270 step-nozzles of width/height (w/h) ratio of 6.6 and a depth of 100 μm onto the top glass piece (Fig. 1a). Stable droplet formation is governed primarily by channel geometry and wetting-controlled droplet breakup. Robust dripping typically requires a sufficiently large nozzle aspect ratio, and a previous study has reported a critical w/h threshold of approximately 2.6 for stable droplet generation (Huang et al., 2023). While higher w/h ratios (e.g., >3.5) may facilitate more stable droplet formation (Xu et al., 2018), excessively wide geometry may lead to droplet formation at multiple locations along the step edge (Wu et al., 2021). Therefore, considering both these design criteria and fabrication constraints imposed by the vendor, a w/h ratio of 6.6 was selected in this work. Previous studies have shown that droplet size in step-emulsification depends primarily on the channel depth and scales approximately linearly (Schuler et al., 2015; Dangla et al., 2013); therefore, a channel depth of 100 μm was selected to target droplets on the order of a few hundred micrometers. These droplets would subsequently solidify to produce microparticles of similar order of magnitude in size that have favorable particle attributes for downstream processing such as flowability and bulk density. While the channel geometries can

2.1. Fabrication of Glass Step-Emulsification Device

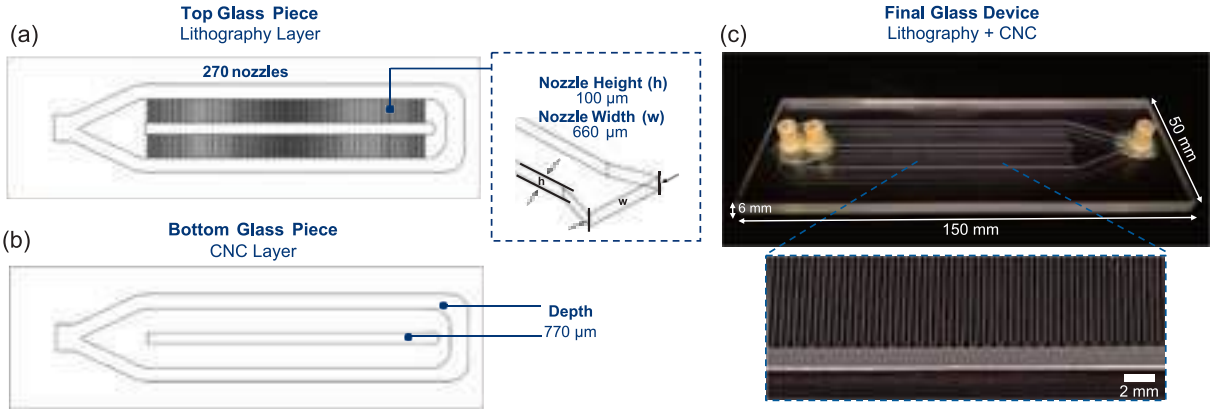

Fig. 1. Glass step-emulsification device feature sizes (not drawn to scale). (a) Top and (b) bottom piece of the device. (c) Isometric view of glass chip device after thermal bonding of the CNC and lithography layers.

be further optimized for specific applications, the present design outlines a canonical system used to demonstrate the feasibility of scalable droplet generation platform. Computer numerical control (CNC) machining was employed to embed deep channels on the bottom glass piece at a depth of 770 µm, as shown in Fig. 1b. The two glass substrates were subsequently thermally bonded together, after which three inlet/outlet holes measuring 1.5 mm were drilled onto the top surface of the chip. PEEK fittings were attached to the surface of the chip using epoxy adhesive, which enabled PTFE tubing (outer diameter: 1.6 mm; inner diameter: 1 mm) to be connected during the operation, as illustrated in Fig. 1c. The fabrication processes described above were performed by Wen Hao Microfluidics (Suzhou, China).

2.2. Treatment of the glass microfluidic device

Surface treatment of step-emulsification devices is essential to ensure stable and reliable droplet generation. Prior to operation, the device was treated with air plasma (Covance-1MP Plasma Machine, South Korea) at a pressure of 0.667 Pa and a power of 150 W for 90 s to remove surface contaminants and increase surface hydrophilicity. Following the plasma treatment, the inner channels of the device were soaked in a 1 M sodium hydroxide (NaOH) solution for 30 min. After flushing the channels with deionized water to remove any residual NaOH solution, the inner channels were soaked with the continuous phase, described in section 2.3, for 30 min prior to use.

2.3. Reagent preparation for step-emulsification

Polyvinyl alcohol (PVA, Mowiol 8–88, MW ~ 67,000 g mol-1), dimethyl carbonate (DMC, ReagentPlus, 99%), ethyl acetate (EA, anhydrous, 99.8%), and methyl ethyl ketone (2-butanone or MEK, ACS reagent, 99.0%) were purchased from Sigma-Aldrich and used as received. While the results presented in this study are based on DMC as a model solvent, a comparative analysis of droplet generation using pharmaceutically relevant solvents (DMC, EA, and MEK) is provided in the Supplementary Information (Fig. S2). FLP (F9677) was purchased from TCI and used as received. 1 kg of HPMCAS medium grade (AQOAT®) was provided as a sample by Shin-Etsu (Japan). For this study, all references to FLP and HPMCAS without additional qualifiers pertain to their as-received state, unless otherwise noted. Ultrapure water (18.3 MΩ) was obtained from a Sartorius Arium Pro Ultrapure water purifier. The dispersed phase was prepared by co-dissolving FLP and HPMCAS at concentrations of 1% w/v and 4% w/v, respectively, in water-saturated DMC. The resulting mixture was stirred for 1 h before use and is referred to as 20% FLP-HPMCAS. Here, 20:80 FLP:HPMCAS refers to 20 wt% FLP and 80 wt% HPMCAS relative to the total solid content. The final mixture appears slightly turbid due to partially suspended HPMCAS particles; although this does not affect the emulsion generation process in the glass chip, further characterization of the DP can be found in the Supplementary Information (Fig. S1). An aqueous continuous phase contains 1.5% w/v of PVA as a surfactant in ultrapure water to stabilize oil-in-water emulsions.

2.4. Synthesis of ASD particles

To ensure continuous droplet generation, both the disperse and continuous phases were pumped using peristaltic pumps (Lead Fluid BT 100S-1, China) instead of using batch-wise syringe pumps. L/S 14 precision pump tubing from VWR was used to pump liquids from the reagent reservoirs, while PTFE tubing (ID: 1.0 mm and OD: 1.6 mm) connected the pump tubing to the fittings on the glass device. The dispersed and continuous phases were infused at a flowrate of 0.9 and 4.5 mL/min, respectively, unless otherwise specified. The emulsification process was monitored using a high-speed camera (Ametek Phantom C110, USA) to ensure monodisperse droplet formation in the dripping regime. The generated emulsion droplets were transported via a PTFE outlet tube into a custom glass column (SG Labware Pte Ltd, Singapore) with a dimension of 15 x 70 cm (diameter x height). The column enables complete antisolvent extraction of the droplets while gravity assists particle settling. Homogenous mixing within the column was maintained by using a digital overhead stirrer (VOS 40, VWR), operating at a mild stirring speed of 30 rpm with an anchor-blade stirrer shaft. Initially, 2.5 L of ultra-pure water was added to the column. During operation, ultra-pure water was continuously pumped into the glass column at a flowrate of 15.5 mL/min to maintain a steady-state solvent concentration of 7% v/v within the column to drive antisolvent extraction. The suspension of fully solidified FLP-HPMCAS microparticles was collected at the bottom of the glass column and subsequently washed with ultrapure water and dried overnight under vacuum at room temperature (~25 ℃) prior to further characterization.

2.5. Solid-state outcome and particle characterisation

To confirm that 20% FLP-HPMCAS microparticles are amorphous, powder X-ray diffraction (PXRD) and differential scanning calorimetry (DSC) were performed to detect any signs of crystallinity.

The PXRD analysis was performed with a diffractometer (Bruker D8 Advanced, USA) that used Cu radiation with a wavelength of 1.54 Å,

operated at a voltage of 40 kV, current of 30 mA, and scanning rate of 0.78°/min over a 2θ range of 5 − 40°. Modulated differential scanning calorimetry (mDSC) was performed using a DSC25 apparatus (TA Instruments, USA). Approximately 5 mg of sample was sealed in a Tzero aluminum hermetic pan with a pinhole, and an empty pan of the same type was used as the reference. The sample was first equilibrated at 20 °C, followed by temperature modulation with an amplitude of ± 0.32 °C and a period of 60 s. After an isothermal hold for 10 min, the sample was heated from 20 to 200 °C at an underlying heating rate of 2 °C/min under a dry nitrogen purge at 50 mL/min. The glass transition temperature was determined from the reversing heat-flow signal. A reference was established using an empty crimped pan with a pinhole, and dry nitrogen with a flowrate of 50 mL/min was used as the purge gas. Particle morphology was examined using field-emission scanning electron microscopy (FESEM; JEOL JSM-7610F Plus, USA) operating at 5 kV. FESEM samples were prepared on conventional AISI 316 L stainless steel electron microscopy stubs using carbon tape and sputter-coated with ~ 10 nm of platinum for resolution enhancement. Particle size distributions were measured using a Mastersizer 3000E (Malvern Panalytical, Netherlands) with a non-spherical model. Particles were added until obscuration was between 1–5%. A stirring speed of 2000 rpm was used. Refractive indices of 1.3 were used for HPMCAS and 20% FLP-HPMCAS, respectively, and 1.6 was used for FLP.

2.6. Powder rheology characterization

Bulk density was measured to assess the amount of powder that can be loaded into a confined volume, such as the hopper of a tablet press. Raw FLP and 20% FLP-HPMCAS powders were loaded into a pre-tared 5 mL graduated cylinder up to the 5 mL mark, and the mass was recorded using an analytical weighing scale (Mettler Toledo, UK). Power flow properties relevant to solid dosage forms were also evaluated using shear cell tests with an FT4 powder rheometer (Freeman Technology, UK). Powders were loaded into a 1 mL cylindrical shear cell and conditioned prior to testing. The powder bed was then pre-consolidated at a normal stress (σ) of 3 kPa using a vented piston to mimic pharmaceutical processes where most operations are carried out below 6 kPa (Clancy, 2017). Incipient shear stresses for flow were determined at normal stresses of 1, 1.25, 1.5, 1.75, and 2 kPa with a bladed shear head. The inbuilt FT4 analysis software was used to plot a yield locus based on the recorded values of shear stress and normal stress.

2.7. Tabletability of ASD particles

A simple tablet formulation was prepared to demonstrate the potential of the ASD powders produced for marketable solid dosage forms. Each tablet contained 17 wt% ASD powder, 81 wt% Microcrystalline Cellulose (MCC; PH102 Avicel from Sigma-Aldrich) and 2 wt% Crospovidone (Kollidon CL, BASF, Germany), all of which were used as received. MCC served as the filler, while crospovidon acted as a tablet disintegrant to aid burst release of amorphous FLP. Tablets weighing 150 mg each, corresponding to 5 mg FLP per tablet, were produced using a compaction simulator (Styl'One, Medelpharm, France) fitted with an 8 mm flat-face punches and die set (Natoli Engineering, USA). Compression was carried out at predetermined pressures using a compression speed of 60 mm/s, followed by tablet ejection at an ejection speed of 90 mm/s. The tablet tensile strength was calculated based on the tablet hardness measured using a hardness tester (TBF1000, Copley Scientific, UK), tablet diameter and thickness.

2.8. Drug loading and tablet dissolution

Drug loading of the FLP-HPMCAS microparticles was measured by dissolving 5 mg of microparticles in 5 mL ethanol (ACS reagent, ≥99.5%) under 30 min of sonication. The resulting solution was filtered through a 0.22 μm PTFE filter and diluted with ethanol prior to analysis. FLP concentration was measured using a Cary 60 UV–visible spectrophotometer and a calibration curve was constructed with known concentrations of FLP in ethanol at a 364 nm wavelength. *In vitro* dissolution testing was performed on tablets consisting of ASD microparticles using USP 2 dissolution apparatus (paddle) (Caleva 9ST Dissolution Tester, Germany). The dissolution was carried out in 900 mL phosphate buffer (pH 7.4) maintained at 37 °C with a paddle speed of 100 rpm. Aliquots were withdrawn at predetermined time interval, and FLP concentration in the dissolution medium was determined using high-performance liquid chromatography (HPLC). The mobile phase consisted of acetonitrile: methanol: buffer in a ratio of 2: 1: 2, eluted at 1 mL/min. The buffer was prepared by adding 8 mL of 1 M phosphoric acid to a solution of 6.9 g monobasic sodium phosphate and diluted with water to 1 L. A reversed-phase C-18 column (ACE Generix, 5 μm, 4.6 mm × 150 mm, Advanced Chromatography Technologies, UK) was used as the stationary phase and maintained at 40 °C. A 20 μL sample was injected into the column for each run and FLP detected at 254 nm. The crystalline solubility of FLP in pH 7.4 phosphate buffer was determined by equilibrating excess crystalline FLP in the buffer at 37 °C, followed by filtration and HPLC quantification of the dissolved FLP concentration.

3. Results and discussion

3.1. High-throughput production of ASD particles in a continuous antisolvent extraction column

Fig. 2 illustrates the integrated platform for continuous production of ASD microparticles, combining step-emulsification with downstream antisolvent extraction. The process configuration (Fig. 2a) consists of four independently controlled flow streams that enable continuous delivery of the dispersed, continuous, extraction and harvesting phases. Highly monodisperse oil-in-water (O/W) droplets are generated within the glass step-emulsification device as show in Fig. 2b, with the corresponding phase compositions and operating flowrates summarized in Fig. 2c.

The glass chip device includes a central deep channel (870 μm) for the dispersed phase and two parallel deep channels located at the ends for the continuous phase. The central channel symmetrically branches into a series of shallow channels (100 μm tall) with wedge-shaped nozzles on both sides, through which the dispersed phase flows into the distal deep channels carrying the continuous phase. With appropriate surface treatment, the hydrophilicity of the glass surfaces is enhanced, promoting preferential wetting by the continuous phase (Eggersdorfer et al., 2018) and enabling stable droplet generation. Under suitable combinations of dispersed and continuous phase flowrates, the system operates in a dripping regime to produce highly monodisperse droplets. While a canonical system is presented in this paper, an analysis of operation at different flowrates using various pharmaceutical solvents can be found in the Supplementary Information (S2).

The dispersed phase contains co-dissolved FLP and HPMCAS in water-saturated DMC at 5% w/v solid loading/saturated DMC, while the continuous phase contains 1.5% w/v PVA/ultrapure water with 10% v/v DMC/ultrapure water. FLP was chosen as a model API due to its low solubility in its crystalline form, and HPMCAS was chosen as a model excipient due to the presence of acetyl and succinyl moieties (Butreddy, 2022) with effective precipitation inhibitor properties. This makes HPMCAS an ideal excipient to form amorphous compounds to demonstrate inhibition of recrystallization in dissolution, thereby extending the period of supersaturation (Nguyen et al., 2016) While the glass chip has versatile compatibility with different solvents, dimethyl carbonate (DMC) was chosen as a non-toxic green solvent with good miscibility with water for co-dissolving drugs and excipients (Pyo et al., 2017).

Since water is miscible in DMC at 3.3% v/v (Pyo et al., 2017), extraction can occur in reverse at the DMC-water interface. PVA precipitation in the form of films at the interface has been observed, which

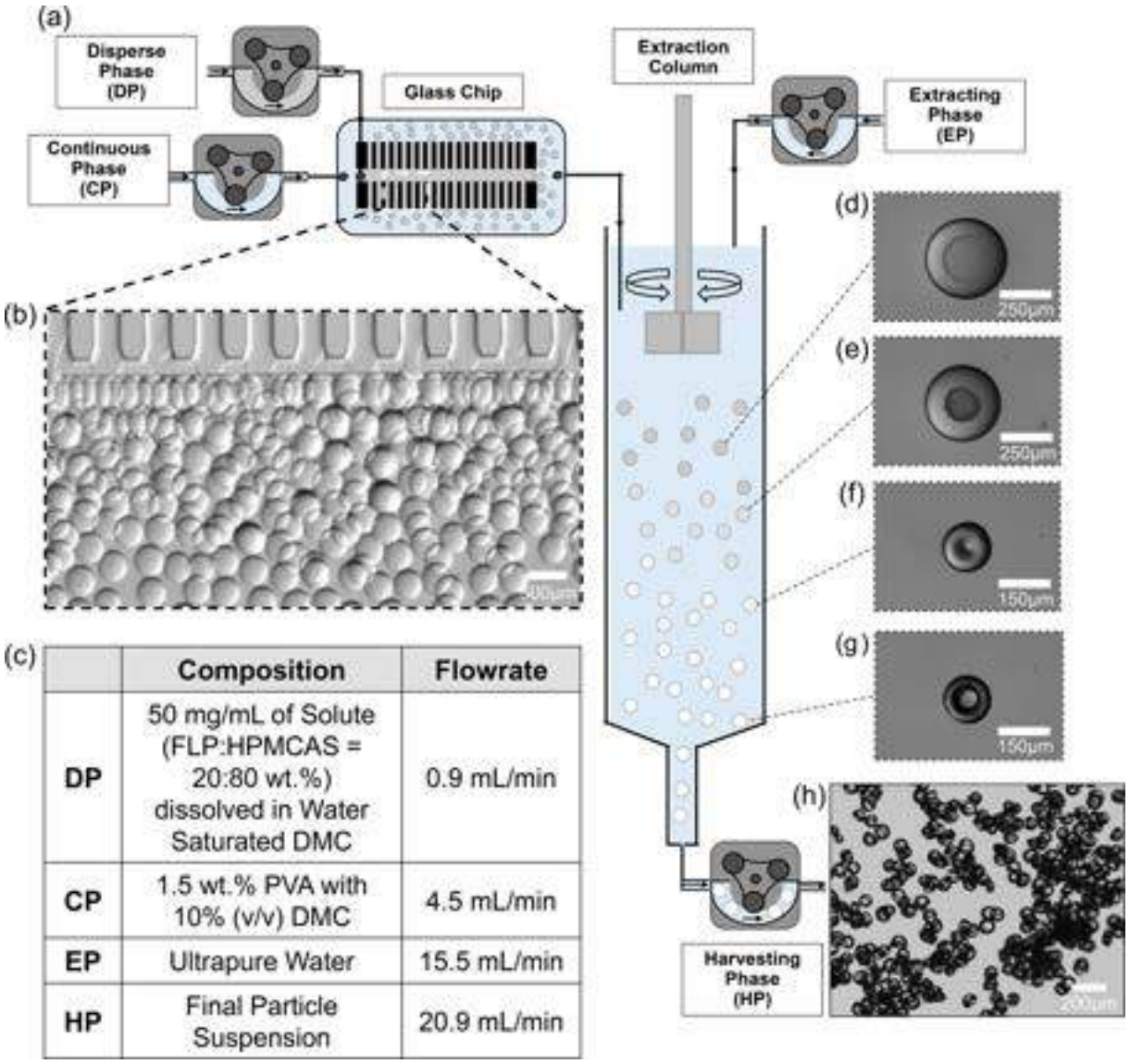

	Composition	Flowrate
DP	50 mg/mL of Solute (FLP:HPMCAS = 20:80 wt.%) dissolved in Water Saturated DMC	0.9 mL/min
CP	1.5 wt.% PVA with 10% (v/v) DMC	4.5 mL/min
EP	Ultrapure Water	15.5 mL/min
HP	Final Particle Suspension	20.9 mL/min

Fig. 2. Emulsion droplet generation and continuous antisolvent extraction. (a) The setup is comprised of 4 peristaltic pumps, a step-emulsification glass chip, and a glass extraction column (length = 70 cm and diameter = 7.5 cm) with an overhead stirrer at 30 rpm. (b) Generation of emulsion droplet inside a glass chip (c) Table of different compositions and flowrates for 4 flow phases. (d-g) Evolution of emulsion droplets along the extraction column at every 10 cm interval down from the exit nozzle. Images were captured using a high-speed camera. (h) Fully extracted particles in suspension were imaged using brightfield microscopy.

we hypothesized to arise from water migration from PVA solution *into* droplets of the dispersed phase, leading to high local PVA concentrations. To prevent PVA precipitation during the emulsification process, both the dispersed and continuous phases were mutually saturated; thus, for the combination of DMC and 3% PVA in water, DMC is saturated with water, and vice versa, to maintain equilibrium during the emulsification process.

The extraction column of 7.5 cm in diameter and 70 cm in length initially contains 2.5 L of ultrapure water, which is subsequently replenished by the dispersed and the continuous phase during the operation. The extraction phase is infused to maintain the steady-state solvent concentration of 7% v/v inside the glass column and the rate of particle collection is fixed to maintain the liquid level 10 cm from the top for steady-state operation. With 20% overhead height for safety, the emulsion droplets are introduced at a depth of 15 cm from the top of the glass column, with a typical residence time of 3 min before they reach the bottom. The injection height is sufficient to ensure complete extraction and solidification of the emulsion droplets through the steady-state solvent-antisolvent concentration gradient as well as the convection induced by an overhead stirrer run at 30 rpm and gravity. The evolution of emulsion droplets along the column height is captured in Fig. 2d-g, after collecting the emulsion droplets at different column heights and subsequent immediate imaging using a high-speed camera. The top-down images of the emulsion droplets highlight the gradual droplet shrinkage and solidification that eventually yield buckled particles at the bottom of the extraction column. The buckling of emulsion droplets under falling anti-solvent extraction has also been observed by Remigijus et al. who proposed that anisotropic droplet shrinkage due to convection causes semisolids to buckle during the extraction window (Vasiliauskas et al., 2015). Further investigation and optimization can be conducted for this extraction process about the column geometry, residence time, and the solvent-antisolvent concentration gradient inside the glass column; we leave these studies to a future contribution.

3.2. Microparticle morphology and monodispersity

ASD microparticles were observed using FESEM after isolation and drying, as shown in Fig. 3. Fig. 3a and 3b show highly monodisperse

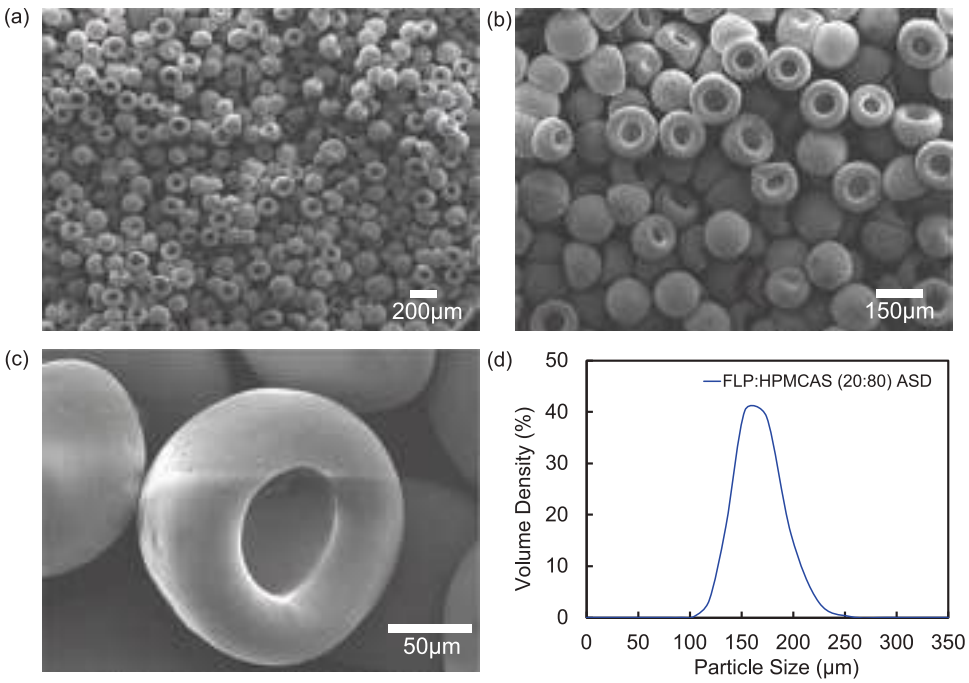

Fig. 3. FESEM images and particle size distribution of ASD particles. (a-c) FESEM image of FLP-HPMCAS microparticles at 35, 85, and 450X magnification. (d) Particle size distribution (volume density vs. size) of FLP-HPMCAS microparticles measured using laser diffraction in suspension.

particles in bulk, demonstrating excellent control over particle size and morphology, which is typically challenging to achieve with conventional powders that are often polydisperse and exhibit poor powder rheology. Fig. 3c not only depicts a buckled morphology of co-processed ASD microparticles but also demonstrates no visible crystalline growth of FLP on the HPMCAS surface, which provides additional evidence for the amorphous characterization presented in the next section. An excellent size distribution of ASD microparticles is further supported by the static light scattering measurement result shown in Fig. 3d, which illustrates the volume density of suspended microparticles across a wide size range. The average particle diameter (d50) was found to be 163 μm and the 90th (d90) and 10th (d10) percentile of the distribution were found to be 195 and 137 μm respectively. The span value, defined as (d90-d10)/d50 is used to quantify the breadth of the particle size distribution, with a threshold value of 1, beyond which particles are regarded as polydisperse (Wan et al., 2021). While raw powders indeed show span values greater than 1, our co-processed ASD microparticles have a span value of 0.35, indicating remarkable monodispersity. In addition, the co-processed ASD microparticles exhibited a bulk density of 0.313 g/mL, which is notably higher than those of ASDs produced by various methods documented in the existing literature, with bulk densities of 0.194 g/mL (Honick et al., 2020) and 0.230 g/mL (Frank et al., 2022) with the d10 of 2.7 and 9.9 μm, d50 of 10.9 and 27.8 μm and d90 of 30.9 and 61.0 μm respectively. The span values for each sample are 2.59 and 1.84, indicating substantial polydispersity in the samples and far exceeding that of the monodisperse control we have with a span of 0.35 through the microfluidic enabled process. Such an increase in bulk density can be attributed to the improvement in particle morphology conducive to random-close packing and will be beneficial in pharmaceutical manufacturing due to its significant influence on flow, packing, and powder processing. The flow factor of raw FLP using a shear cell measurement was deduced as 3.3, whereas the flow factor of co-processed microparticles was measured as 4.8. As per powder flow classification in the literature (Schulze, 2014), FLP is classified as a 'cohesive' powder, whereas the co-processed microparticle is classified as 'easy flowing', and hence more favorable to the downstream manufacturing process. Key particle attributes are summarized in the Supplementary Information S9.

3.3. ASD solid state outcome

While SEM images provide visual evidence of no crystalline FLP on the co-processed microparticles, further characterization using PXRD and DSC was conducted to confirm their amorphous nature. This is especially important for drugs with low solubility to improve their therapeutic efficacy (Arshad et al., 2021). Modulated differential scanning calorimetry (mDSC) was used to identify the glass transition temperature of the drug-excipient microparticles. As shown in Fig. 4a, raw FLP exhibits a strong melting endotherm at 149 °C, indicating its crystalline nature; however, no melting endotherm was observed for co-processed microparticles. A glass transition temperature (T_g) of approximately 75 °C was observed in the reversing heat-flow signal, supporting the formation of an amorphous drug-polymer dispersion. Residual moisture in the dried 20:80 FLP microparticles was measured by Karl Fischer titration and found to be 0.76 ± 0.10 wt% based on four replicate measurements. While residual water can plasticize HPMCAS and influence the measured T_g, the relatively low residual moisture content is expected to contribute only modestly to the T_g depression based on prior literature (Patel et al., 2022). PXRD analysis further supports these findings. As shown in Fig. 4b, raw FLP exhibit distinct crystalline peaks corresponding to the polymorphic Form I (Guo et al., 2020). In contrast, 20% FLP-HPMCAS microparticles showed no detectable crystalline FLP peaks within the sensitivity of the PXRD method. Prior literature indicates that conventional solid-state techniques such as PXRD and DSC typically have crystallinity detection limits on the order of 1–5 wt% in ASDs (S'Ari et al., 2021). Because no separate sensitivity study was conducted in this work, we acknowledge that trace levels of crystallinity below the method sensitivity cannot be excluded. Nevertheless, the combined PXRD and mDSC results strongly support an amorphous solid-state outcome for the processed microparticles. In addition, a residual solvent analysis was performed on the dried 20% FLP-HPMCAS microparticles using an Agilent 6890 headspace gas chromatograph. In all triplicate samples the residual dimethyl carbonate was found below the device reporting limit of 0.05% (w/w). In all

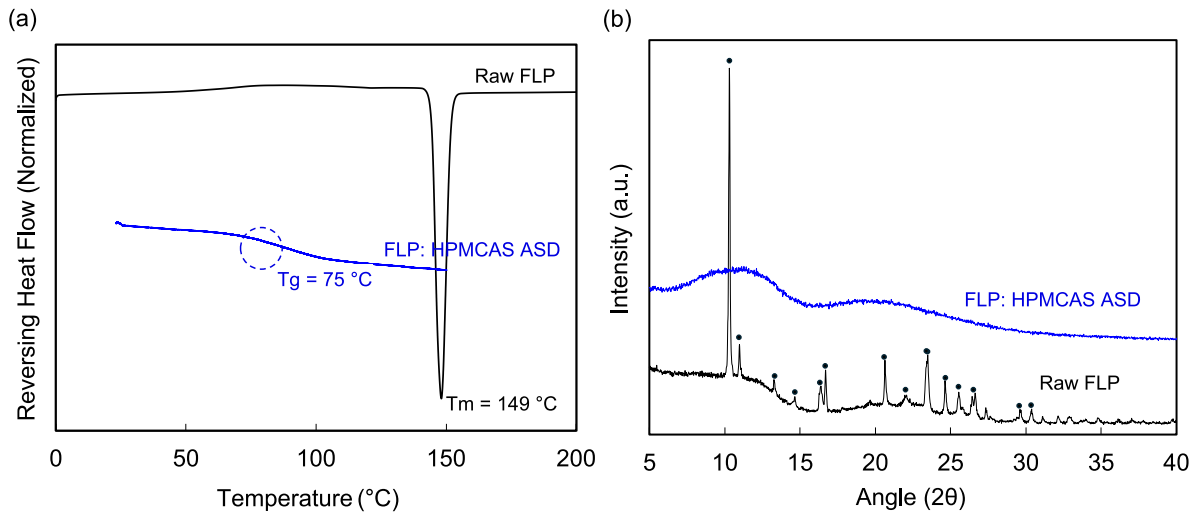

Fig. 4. Solid-state characterization for raw FLP and FLP-HPMCAS (20:80) (a) Normalized DSC thermograms, adjusted to emphasize curve shapes, revealing the presence and absence of exothermic and endothermic peaks in the microparticles. Glass transition Temperature was observed at 75 °C for FLP-HPMCAS (20:80) (b) PXRD spectra of 20% FLP-HPMCAS microparticles, demonstrating amorphous nature evidenced by the absence of crystalline peaks as compared to raw crystalline FLP.

triplicate samples, residual DMC was below the method reporting limit of 0.05% w/w. Although DMC is not specifically listed in ICH Q3C(R9), this reporting limit is ten-fold lower than the general 0.5% w/w concentration threshold applied to Class 3 residual solvents (I.G.F.R.S. Q3C (R9), 2024).

3.4. Tabletting – tensile strength and dissolution

To evaluate downstream processibility, co-processed ASD microparticles were compressed into tablets and their mechanical and dissolution properties were assessed. Based on recommended dosing guidelines for FLP (2.5–10 mg) (Whelton et al., 2017), a target dosage of 5 mg per tablet was chosen. Industrial-grade microcrystalline cellulose (MCC, Avicel-PH102) was chosen as a secondary filler, as it is known for its excellent binding property (Albers et al., 2006); and Kollidon CL was chosen as a super disintegrant (Nazmi et al., 2013) to supplement tablet disintegration for amorphous solid dispersions to deliver their therapeutical effect. The tablet formulation used here was designed as a simple proof-of-concept formulation to demonstrate incorporation of the co-processed FLP microparticles into an oral solid dosage form. Fig. 5a demonstrates that intact tablets can be formed even at a relatively low compaction pressure of 50 MPa, without common tablet defects such as capping or lamination. Fig. 5b provides visual evidence of both ASD microparticles and MCC filler are discernibly close to their original shapes at a low compaction pressure of 50 MPa. However, at a higher compaction pressure of 300 MPa in Fig. 5(c and d), MCC seemed to have undergone considerable plastic deformation with enhanced interparticle bonding that resulted in a densified powder bed structure.

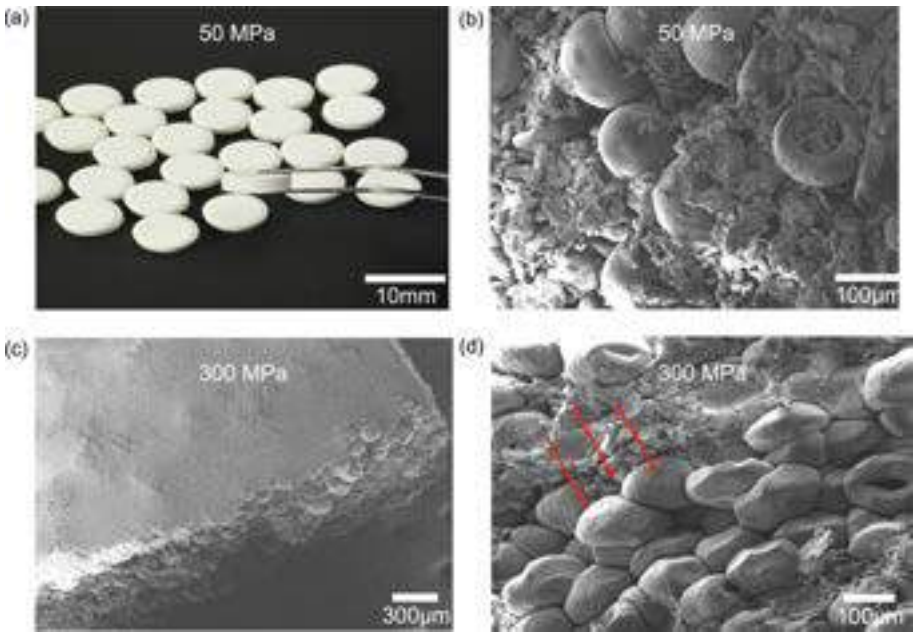

Fig. 5. FESEM images of FLP-HPMCAS microparticles in tablet formulation with respective compaction pressure annotated on each image (a) Image of final tablet formulation with 5 mg FLP dosage, balanced with 81 wt% MCC and 2 wt% Kollidon. (b) FESEM image of the cross-section of the ASD tablet compacted at 50 MPa. (c) FESEM image of the ASD tablet compacted at 300 MPa (top-down view) (d) Cross-sectional FESEM image of an ASD tablet compacted at 300 MPa with the direction of compaction represented in red arrows.

While ASD microparticles also show signs of plastic deformation perpendicular to the direction of the compaction force, they remained discernible within the compact and underwent limited morphological deformation after compression. This suggests that the microparticles can be incorporated into the tablet matrix without complete collapse of their particle morphology. However, further studies using different tablet formulations would be required to isolate the intrinsic contribution of the ASD microparticles to tablet mechanical properties, which is beyond the scope of the present study.

As shown in Fig. 6a, tablet tensile strength increases with compression pressure up to 200 MPa, beyond which it plateaus. This could be attributed to MCC's property to readily undergo plastic deformation (Hentzschel et al., 2011) since it comprises the bulk of the tablet mass. Therefore, the tensile strength results should not be interpreted as the intrinsic tabletability of the ASD microparticles alone; rather, these results demonstrate that the co-processed FLP microparticles can be incorporated into a conventional MCC-based tablet formulation, which can sufficiently satisfy the industrial standard for tablet tensile strength between 1.7 and 2 MPa (Sabri et al., 2018). *In vitro* dissolution testing of the compacted tablets is shown in Fig. 6b. The dissolution experiment was conducted under non-sink conditions with respect to crystalline FLP. Based on the crystalline FLP solubility of 0.0008 mg/mL, a dissolution volume of 900 mL, and an FLP dose of 5 mg per tablet, the sink index was calculated as 0.144. These non-sink conditions were selected to enable evaluation of apparent supersaturation generation and maintenance from the ASD tablet formulation, instead of measuring complete drug release under highly dilute sink conditions. Raw FLP tablets, which were prepared with the same total tablet mass, FLP dose, and excipient composition as the ASD tablets, exhibit slow and gradual dissolution profile due to their low aqueous solubility in its crystalline form (Kanaujia et al., 2015) with the solubility limit of 0.8μ g/mL. In contrast, ASD tablets containing co-processed FLP microparticles displayed an initial burst release, reaching an apparent supersaturation concentration of approximately 2.5 μg/mL that was maintained over the measured dissolution period. This behavior can be interpreted within the spring-and-parachute framework commonly used to describe ASD dissolution, where rapid release from the amorphous formulation generates transient supersaturation and the polymer helps maintain the supersaturated state by inhibiting drug precipitation and/or crystallization (Hiew et al., 2021).. Because the amorphous solubility and LLPS onset concentration of FLP were not directly measured, the observed concentration is reported as an apparent supersaturation level under the present non-sink dissolution conditions, rather than being assigned to the amorphous solubility limit or definitive formation of a drug-rich phase. In contrast, raw FLP tablets exhibited slower and more gradual dissolution because crystalline FLP is limited by its low aqueous solubility and crystal dissolution kinetics. These results demonstrate that the co-processed FLP microparticles retain enhanced dissolution performance even after incorporation into a tablet formulation, while long-term storage stability remains an important subject for future study.

4. Conclusion

This study introduces an advanced alternative to the traditional methods employed for ASD production in the pharmaceutical sector. The end-to-end process presented in this study enables the fabrication of ASD microparticles through solvent-templated droplet microfluidics using step emulsification. This platform yields monodisperse droplets from various industrially-relevant solvent systems; a model solvent dimethyl carbonate was demonstrated in this paper to produce amorphous FLP using HPMCAS as a co-excipient. The work also demonstrates a successful implementation of the continuous extraction column to seamlessly extract the emulsion droplets through gravitational settling. The analogous nature of the extraction column to many industrial equipment eases the potential adaption and scale-up. By avoiding fine formation through precise particle engineering and designing an extraction process using anti-solvent in which both the drug and excipient exhibit negligible solubility, the process intrinsically minimizes mass loss during the production. This contrasts with particles produced by conventional ASD manufacturing methods such as spray drying, which can exhibit broad particle-size distributions, irregular morphology, low bulk density, and poor powder flowability, often requiring additional downstream processing to improve handling and tableting performance. Although a full end–to–end industrial–scale filtration and drying process is beyond the scope of this work, we expect that integrating our demonstrated approach with standard industrial downstream operations could achieve higher steady–state yields than conventional methods. From an environmental sustainability perspective, the present process benefits from the use of dimethyl carbonate as a model solvent, which has been described as a greener alternative to several conventional organic solvents, and from the use of water as the antisolvent. However, the overall sustainability of the platform will depend strongly on solvent and antisolvent recovery at larger scale. A full life-cycle assessment, including solvent recovery efficiency and waste generation will be important for future scale-up. In addition, we showcase end-to-end characterization from powder to final oral dosage form, which clearly demonstrate that our highly monodispersed ASD microparticles exhibit robust performance even in the final dosage form. The dissolution profile of ASD tablets shows a promising outcome to improve the bioavailability of many poorly soluble drugs. Overall, our results highlight the potential to bridge the gap between microfluidic precision and practical pharmaceutical manufacturing.

CRediT authorship contribution statement

Jun Ho Min: Writing – review & editing, Writing – original draft,

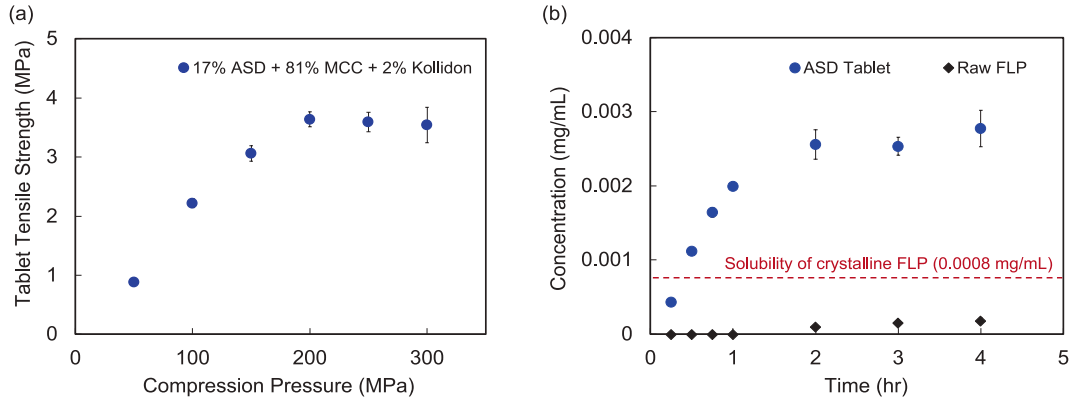

Fig. 6. Tablet tensile strength and tablet dissolution of ASD microparticles. (a) Resulting tablet tensile strength at different compression pressures. (b) The dissolution profile of ASD tablet produced at 200 MPa (maximum tensile strength) compared against the dissolution profile of raw crystalline FLP in pH 7.4 PBS solution.

Visualization, Validation, Methodology, Investigation, Formal analysis, Data curation, Conceptualization. **Zheng Jie Liew:** Writing – original draft, Visualization, Methodology, Investigation, Formal analysis, Data curation, Conceptualization. **Leon Yoon Ho:** Validation, Methodology, Investigation, Formal analysis, Data curation. **Zhi Kai Tio:** Validation, Methodology, Investigation, Data curation. **Arif Z. Nelson:** Validation, Methodology, Conceptualization. **Natalia Veronica:** Methodology, Formal analysis, Data curation. **Lai Wah Chan:** Writing – review & editing, Resources, Formal analysis. **Paul Wan Sia Heng:** Supervision, Resources, Formal analysis. **Abigail Gershman:** Methodology, Data curation. **Samir Kulkarni:** Validation, Investigation, Formal analysis. **John Richard Murphy:** Validation, Investigation, Formal analysis. **Jennifer Ann Dolman:** Validation, Investigation, Formal analysis. **Catherine Michelle Ambler:** Supervision, Investigation, Formal analysis. **Shawn LaCasse:** Resources, Formal analysis. **Kapildev Arora:** Validation, Formal analysis. **Saif A. Khan:** Writing – review & editing, Validation, Supervision, Project administration, Investigation, Funding acquisition, Formal analysis, Conceptualization. **Patrick S. Doyle:** Writing – review & editing, Supervision, Resources, Project administration, Methodology, Funding acquisition, Conceptualization.

Declaration of competing interest

The authors declare the following financial interests/personal relationships which may be considered as potential competing interests: Patrick S. Doyle reports financial support was provided by Pfizer Inc. If there are other authors, they declare that they have no known competing financial interests or personal relationships that could have appeared to influence the work reported in this paper.

Acknowledgments

This research was funded by Pfizer Asia Manufacturing. The authors thank Dr. Bryan Li, and Dr. Eunice Yeap from Pfizer for providing an industry perspective to the research project. Dr. Swati Shikha from the Singapore-MIT Alliance for Research and Technology (SMART) for the guidance on the initial stages of making cPADs, Dr. Purnima Manghnani from SMART for the fruitful discussions on troubleshooting process bottlenecks at the droplet generation stage, and Dr. Ariel Chua from the National University of Singapore for the equipment support.

Appendix A. Supplementary data

Further information on HPMCAS suspension, different solvent systems, PLM, calibration data for spectrometry, and tablet images. Supplementary data to this article can be found online at https://doi.org/10.1016/j.ijpharm.2026.127193.

Data availability

Data will be made available on request.

References

Agrawal, A., Dudhedia, M., Zimny, E., 2015. Hot melt extrusion: development of an amorphous solid dispersion for an insoluble drug from mini-scale to clinical scale. AAPS PharmSciTech 17. https://doi.org/10.1208/s12249-015-0425-7.

Albers, J., Knop, K., Kleinebudde, P., 2006. Brand-to-brand and batch-to-batch uniformity of microcrystalline cellulose in direct tableting with a pneumohydraulic tablet press. Pharmazeutische Ind. 68, 1420–1428.

Amstad, E., Chemama, M., Eggersdorfer, M., Arriaga, L., Brenner, M., Weitz, D., 2016. Robust scalable high throughput production of monodisperse drops. Lab Chip 16. https://doi.org/10.1039/C6LC01075J.

Arshad, S., Zafar, S., Yousef, B., Alyassin, Y., Ali, R., AlAsiri, A., Chang, M.-W., Ahmad, Z., Elkordy, A., Faheem, A., Pitt, K., 2021. A review of emerging technologies enabling improved solid oral dosage form manufacturing and processing. Adv. Drug Deliv. Rev. 178, 113840. https://doi.org/10.1016/j.addr.2021.113840.

Babu, N., Nangia, A., 2011. Solubility advantage of amorphous drugs and pharmaceutical cocrystals. Cryst. Growth Des. 11, 2662–2679. https://doi.org/10.1021/cg200492w.

Beyer, A., Radi, L., Grohganz, H., Löbmann, K., Rades, T., Leopold, C., 2016. Preparation and recrystallization behavior of spray-dried co-amorphous naproxen-indomethacin. Eur. J. Pharm. Biopharm. 104. https://doi.org/10.1016/j.ejpb.2016.04.019.

Butreddy, A., 2022. Hydroxypropyl methylcellulose acetate succinate as an exceptional polymer for amorphous solid dispersion formulations: a review from bench to clinic. Eur. J. Pharm. Biopharm. 177. https://doi.org/10.1016/j.ejpb.2022.07.010.

Chong, Z.Z., Hwa Tan, S., Gañán-Calvo, A., Tor, S., Loh, N., Nguyen, N.-T., 2015. Active droplet generation in microfluidics. Lab Chip 16. https://doi.org/10.1039/C5LC01012H.

Chu, K., Lee, E., Jeong, S., Park, E.-S., 2012. Effect of particle size on the dissolution behaviors of poorly water-soluble drugs. Arch. Pharm. Res. 35, 1187–1195. https://doi.org/10.1007/s12272-012-0709-3.

Clancy, D., 2017. Continuous secondary process selection and the modeling of batch and continuous wet granulation, in: Predictive Modeling of Pharmaceutical Unit Operations, pp. 343–381. 10.1016/B978-0-08-100154-7.00013-2.

Dangla, R., Fradet, E., Lopez, Y., Baroud, C., 2013. The physical mechanisms of step emulsification. J. Phys. D Appl. Phys. 46, 114003. https://doi.org/10.1088/0022-3727/46/11/114003.

Eggersdorfer, M., Seybold, H., Ofner, A., Weitz, D., Studart, A., 2018. Wetting controls of droplet formation in step emulsification. In: Proceedings of the National Academy of Sciences 115. https://doi.org/10.1073/pnas.1803644115.

Ekdahl, A., Mudie, D., Malewski, D., Amidon, G., Goodwin, A., 2019. Effect of spray-dried particle morphology on mechanical and flow properties of felodipine in PVP VA amorphous solid dispersions. J. Pharm. Sci. 108. https://doi.org/10.1016/j.xphs.2019.08.008.

Fortt, R., Tona, R., Martin-Soladana, P., Ward, G., Lai, D., Durrant, J., Douillet, N., 2020. Extractive crystallization of cabotegravir in droplet-based microfluidic devices. J. Cryst. Growth 552, 125908. https://doi.org/10.1016/j.jcrysgro.2020.125908.

Frank, D., Punia, A., Fahy, M., Dalton, C., Rowe, J., Schenck, L., 2022. Densifying co-precipitated amorphous dispersions to achieve improved bulk powder properties. Pharm. Res. 39, 1–12. https://doi.org/10.1007/s11095-022-03416-6.

Guo, W., Li, C., Du, P., Wang, Y., Zhao, S., Wang, J., Yang, C., 2020. Thermal properties of drug polymorphs: a case study with felodipine form I and form IV. J. Saudi Chem. Soc. 24. https://doi.org/10.1016/j.jscs.2020.04.003.

Hentzschel, C., Sakmann, A., Leopold, C., 2011. Comparison of traditional and novel tableting excipients: physical and compaction properties. Pharm. Dev. Technol. 17. https://doi.org/10.3109/10837450.2011.572897.

Hiew, T., Zemlyanov, D., Taylor, L., 2021. Balancing Solid-state stability and dissolution performance of lumefantrine amorphous solid dispersions: the role of polymer choice and drug–polymer interactions. Mol. Pharm. XXXX. https://doi.org/10.1021/acs.molpharmaceut.1c00481.

Honick, M., Das, S., Hoag, S., Muller, F., Alayoubi, A., Feng, X., Zidan, A., Ashraf, M., Polli, J., 2020. The effects of spray drying, HPMCAS grade, and compression speed on the compaction properties of itraconazole-HPMCAS spray dried dispersions. Eur. J. Pharm. Sci. 155. https://doi.org/10.1016/j.ejps.2020.105556.

Huang, B., Ge, X., Rubinstein, B.Y., Chen, X., Wang, L., Xie, H., Leshansky, A.M., Li, Z., 2023. Gas-assisted microfluidic step-emulsification for generating micron- and submicron-sized droplets. Microsyst. Nanoeng. 9. https://doi.org/10.1038/s41378-023-00558-4.

I.G.F.R.S. Q3C(R9), 2024. GUIDELINE FOR RESIDUAL SOLVENTS Q3C(R9) - Current step 4 version, Available from: ⟨http://Www.Ich.Org/Fileadmin/Public_Web_Site/ICH_Products/Guidelines/Qual Ity/Q3C_R9/Step4/Q3C_R9_Guideline.Pdf⟩.

Kanaujia, P., Poovizhi, P., Ng, W.K., Tan, R.B.H., 2015. Amorphous formulations for dissolution and bioavailability enhancement of poorly soluble APIs. Powder Technol. 285. https://doi.org/10.1016/j.powtec.2015.05.012.

Kumar, N.S.K., Suryanarayanan, R., 2022. Crystallization propensity of amorphous pharmaceuticals: kinetics and thermodynamics. Mol. Pharm. 19. https://doi.org/10.1021/acs.molpharmaceut.1c00839.

Lee, J., Park, C., Whitesides, G., 2004. Solvent compatibility of poly(dimethylsiloxane)-based microfluidic devices. Anal. Chem. 75, 6544–6554. https://doi.org/10.1021/ac0346712.

Lian, J., Zheng, S., Liu, C., Xu, Z., Ruan, X., 2019. Investigation of microfluidic co-flow effects on step emulsification: wall contact angle and critical dimensions. Colloids Surf A Physicochem Eng Asp 580, 123733. https://doi.org/10.1016/j.colsurfa.2019.123733.

Loo, S., Serguei, S., Kraft, M., Gilet, T., 2016. Droplet formation by squeezing in a microfluidic cross-junction. Microfluid. Nanofluidics 20, 146. https://doi.org/10.1007/s10404-016-1807-1.

Lugtu-Pe, J., Lin, B., Chen, K., Ghaffari, A., Kane, A., Wu, X.Y., 2021. Tailoring release profiles of BCS class II drugs using controlled release amorphous solid dispersion beads with membrane-reservoir design: effect of pore former and coating levels. Mol. Pharm. 18. https://doi.org/10.1021/acs.molpharmaceut.1c00623.

Myślińska, M., Stocker, M., Ferguson, S., Healy, A., 2023. A comparison of spray-drying and co-precipitation for the generation of amorphous solid dispersions (ASDs) of hydrochlorothiazide and simvastatin. J. Pharm. Sci. 112. https://doi.org/10.1016/j.xphs.2023.02.012.

Nazmi, M., Islam, A., Bhuiyan, M., Reza, M., 2013. Effect of superdisintegrants and method of preparation on disintegration time and release profile of carbamazepine from immediate release tablet. J. Appl. Pharm. Sci. 3, 80–84. https://doi.org/10.7324/JAPS.2013.3515.

Ng, D., Nelson, A., Ward, G., Lai, D., Doyle, P., Khan, S., 2022. Control of drug-excipient particle attributes with droplet microfluidic-based extractive solidification enables

improved powder rheology. Pharm. Res. 39, 1–11. https://doi.org/10.1007/s11095-021-03155-0.
Nguyen, M.H., Tran, T.T., Hadinoto, K., 2016. Controlling the burst release of amorphous drug-polysaccharide nanoparticle complex via crosslinking of the polysaccharide chains. Eur. J. Pharm. Biopharm. 104. https://doi.org/10.1016/j.ejpb.2016.05.006.
Ofner, A., Moore, D., Rühs, P.A., Schwendimann, P., Eggersdorfer, M., Amstad, E., Weitz, D., Studart, A., 2016. High-throughput step emulsification for the production of functional materials using a glass microfluidic device. Macromol. Chem. Phys. 218, 1600472. https://doi.org/10.1002/macp.201600472.
Pandi, P., Bulusu, R., Kommineni, N., Khan, W., Singh, M., 2020. Amorphous Solid Dispersions: an update for preparation, characterization, mechanism on bioavailability, stability, regulatory considerations and marketed products. Int. J. Pharm. 586, 119560. https://doi.org/10.1016/j.ijpharm.2020.119560.
Papich, M., Martinez, M., 2015. Applying biopharmaceutical classification system (BCS) criteria to predict oral absorption of drugs in dogs: challenges and pitfalls. AAPS J. 17. https://doi.org/10.1208/s12248-015-9743-7.
Patel, N.G., Banella, S., Serajuddin, A.T.M., 2022. Moisture sorption by polymeric excipients commonly used in amorphous solid dispersions and its effect on glass transition temperature: II. Cellulosic polymers. J. Pharm. Sci. 111. https://doi.org/10.1016/j.xphs.2022.07.020.
Pyo, S.-H., Park, J., Chang, T.-S., Hatti-Kaul, R., 2017. Dimethyl carbonate as a green chemical. Curr. Opin. Green Sustain. Chem. 5. https://doi.org/10.1016/j.cogsc.2017.03.012.
S'Ari, M., Blade, H., Cosgrove, S., Drummond-Brydson, R., Hondow, N., Hughes, L.P., Brown, A., 2021. Characterization of amorphous solid dispersions and identification of low levels of crystallinity by transmission electron microscopy. Mol. Pharm. 18. https://doi.org/10.1021/acs.molpharmaceut.0c00918.
Sabri, A.H., Hallam, C.N., Baker, N.A., Murphy, D.S., Gabbott, I.P., 2018. Understanding tablet defects in commercial manufacture and transfer. J. Drug Deliv. Sci. Technol. 46, 1–6. https://doi.org/10.1016/j.jddst.2018.04.020.
Schneider, T., Burnham, D., VanOrden, J., Chiu, D., 2011. Systematic investigation of droplet generation at T-junctions. Lab Chip 11, 2055–2059. https://doi.org/10.1039/c1lc20259f.
Schuler, F., Schwemmer, F., Trotter, M., Wadle, S., Zengerle, R., Von Stetten, F., Paust, N., 2015. Centrifugal step emulsification applied for absolute quantification of nucleic acids by digital droplet RPA. Lab Chip 15. https://doi.org/10.1039/c5lc00291e.
Schulze, D., 2014. Flow Properties of Powders and Bulk Solids.
Sharratt, W.N., Lee, V.E., Priestley, R.D., Cabral, J.T., 2021. Precision polymer particles by flash nanoprecipitation and microfluidic droplet extraction. ACS Appl. Polym. Mater. 3. https://doi.org/10.1021/acsapm.1c00546.
Shi, J., Wu, B., Zhou, J., Ren, D., Zhang, D., An, C., Wang, J., 2023. One-step rapid preparation of CL-20/TNT co-crystal assembly and spheroidized coating based on droplet microfluidic technology. Def. Technol. 27. https://doi.org/10.1016/j.dt.2022.09.013.
Shikha, S., Lee, Y., Doyle, P., Khan, S., 2022. Microfluidic particle engineering of hydrophobic drug with eudragit E100—bridging the amorphous and crystalline gap. Mol. Pharm. 19. https://doi.org/10.1021/acs.molpharmaceut.2c00714.
Stolovicki, E., Ziblat, R., Weitz, D., 2017. Throughput enhancement of parallel step emulsifier devices by shear-free and efficient nozzle clearance. Lab Chip 18. https://doi.org/10.1039/C7LC01037K.
Strotman, N., Schenck, L., 2021. Coprecipitated amorphous dispersions as drug substance: opportunities and challenges. Org. Process Res. Dev. 26. https://doi.org/10.1021/acs.oprd.1c00380.
Surampalli, G., Kumar, P., Nanjwade, B., Patil, P., 2013. Amorphous solid dispersion method for improving oral bioavailability of poorly water-soluble drugs. J. Pharm. Res. 6, 476–480. https://doi.org/10.1016/j.jopr.2013.04.008.
Vasiliauskas, R., Liu, D., Cito, S., Zhang, H., Shahbazi, M.-A., Sikanen, T., Mazutis, L., Santos, H., 2015. A simple microfluidic approach to fabricate monodisperse hollow microparticles for multidrug delivery. ACS Appl. Mater. Interfaces 7, 14822–14832. https://doi.org/10.1021/acsami.5b04824.
Wan, S., Dai, C., Bai, Y., Xie, W., Guan, T., Sun, H., Wang, B., 2021. Application of multivariate methods to evaluate differential material attributes of HPMC from different sources. ACS Omega XXXX. https://doi.org/10.1021/acsomega.1c03009.
Whelton, P., Carey, R., Aronow, W., Casey, D., Collins, K., Himmelfarb, C., Depalma, S., Gidding, S., Jamerson, K., Jones, D., Maclaughlin, E., Muntner, P., Ovbiagele, B., Smith, S., Spencer, C., Stafford, R., Taler, S., Thomas, R., Williams, K., Wright, J., 2017. ACC/AHA/AAPA/ABC/ACPM/AGS/APhA/ASH/ASPC/NMA/PCNA guideline for the prevention, detection, evaluation, and management of high blood pressure in adults: a report of the American College of Cardiology/American Heart ASSOCIATION task force on clinical practice guidelines. Circulation 138 (2018), e484–e594. https://doi.org/10.1161/CIR.0000000000000596.
Wilson, V.R., Lou, X., Osterling, D.J., Stolarik, D.A.F., Jenkins, G.J., Nichols, B.L.B., Dong, Y., Edgar, K.J., Zhang, G.G.Z., Taylor, L.S., 2020. Amorphous solid dispersions of enzalutamide and novel polysaccharide derivatives: investigation of relationships between polymer structure and performance. Sci. Rep. 10. https://doi.org/10.1038/s41598-020-75077-7.
Wu, J., Yadavali, S., LDH, Issadore, D., 2021. Scaling up the throughput of microfluidic droplet-based materials synthesis: a review of recent progress and outlook. Appl. Phys. Rev. 8, 031304. https://doi.org/10.1063/5.0049897.
Xu, X., Yuan, H., Song, R., Yu, M., Chung, H.Y., Hou, Y., Shang, Y., Zhou, H., Yao, S., 2018. High aspect ratio induced spontaneous generation of monodisperse picolitre droplets for digital PCR. Biomicrofluidics 12. https://doi.org/10.1063/1.5011240.
Yadavali, S., Jeong, H.H., Lee, D., Issadore, D., 2018. Silicon and glass very large scale microfluidic droplet integration for terascale generation of polymer microparticles. Nat. Commun. 9. https://doi.org/10.1038/s41467-018-03515-2.